ADVANCED FUNCTIONAL MATERIALS
www.afm-journal.de

Charge Booster Tags for Controlled Release of Therapeutics from a Therapeutic Carrier

Seoungkyun Kim, Dong Hee Kim, Jinhwan Cho, Jaeyun Kim, and Inchan Kwon**

Injectable hydrogels are promising delivery vehicles for the sustained release of therapeutic proteins. Electrostatic interactions between proteins and hydrogels often increase affinity to decelerate protein release. However, this approach is not suitable for weakly charged proteins. The current study shows that the genetic fusion of a highly charged protein segment (charge booster tag) with proteins can control their interactions with injectable gels. A positive or negative charge booster tag is introduced into urate oxidase (UOX), a therapeutic protein for gout, to generate UOX variants with varying net charges. When a positively-charged injectable hydrogel is used, both the in vitro release rate and in vivo serum half-life of UOX are correlated with the net negative charge. This modified delivery approach results in a serum half-life of over 106 h for the UOX variant, which is substantially longer than that of free UOX (3.3 h). Hence, charge booster tags can be used as a systematic strategy for controlling the release of therapeutic proteins.

1. Introduction

Therapeutic proteins exhibit advantages over chemical drugs for disease treatment because of their high selectivity, fast reaction, and biodegradability;[1] thus, proteins are widely used to treat various diseases, including diabetes,[2,3] gout,[4,5] and cancer.[6,7] The therapeutic protein market is continuously expanding,[8] and the number of approved therapeutic proteins is increasing.[9] However, they often exhibit a short half-life in vivo because of their continuous elimination via several mechanisms, including renal filtration and degradation.[10] Thus, repeated administrations are required, leading to poor patient compliance and an increased economic burden. Therefore, enhancing the serum half-life of therapeutic proteins is critical for developing novel therapeutic strategies and expanding their applicability.

To enhance the serum half-life of therapeutic proteins, biocompatible synthetic or natural hydrogels can be used as delivery vectors.[11–14] A hydrogel is a 3D polymer network with several attractive features for therapeutic protein delivery, as the hydrogel can be modified to improve affinity or to enable encapsulation of therapeutic proteins in an aqueous environment.[15,16] Particularly, injectable hydrogels are suitable candidates for delivering therapeutic proteins because of their simple implantation, biodegradability, and biocompatibility.[17–19] To control the release of a therapeutic protein from hydrogels, specific interactions have been evaluated to increase affinity. For example, therapeutic proteins with a high net charge tightly attach to hydrogels with the opposite charge, which can substantially decrease the release rate of the protein.[20–22] Although such electrostatic interactions are suitable for highly charged therapeutic proteins, the success of this strategy is greatly affected by the intrinsic net charge of the proteins under physiological conditions. Moreover, if the net charge of the therapeutic protein is close to zero, it is difficult to extend the half-life through electrostatic interactions. To overcome this limitation of therapeutic proteins with a small net charge, alternative interactions have been investigated. To utilize ligand-specific interactions, albumin ligands (fatty acids or albumin affibodies) were conjugated to either the hydrogel or therapeutic protein, which significantly enhanced the in vivo half-life.[23,24] However, these strategies have several limitations, such as additional conjugation steps and reduced efficacy of the therapeutic protein following conjugation. In addition, specific materials should be introduced to interact with the ligand, resulting in poor versatility. Therefore, a more general approach that does not require complicated processing and can be applied to most therapeutic proteins is needed.

Herein, we investigated a strategy for controlling electrostatic interactions between a charged hydrogel and therapeutic

S. Kim, J. Cho, I. Kwon
School of Materials Science and Engineering
Gwangju Institute of Science and Technology (GIST)
61005, Gwangju, Republic of Korea
I. Kwon
Research Center for Innovative Energy and Carbon Optimized Synthesis for Chemicals (Inn-ECOSysChem)
Gwangju Institute of Science and Technology (GIST)
Gwangju 61005, Republic of Korea
E-mail: inchan@gist.ac.kr
D. H. Kim, J. Kim
School of Chemical Engineering
Sungkyunkwan University (SKKU)
16419, Suwon, Republic of Korea
J. Kim
Department of Health Sciences and Technology
Samsung Advanced Institute for Health Sciences & Technology (SAIHST)
Sungkyunkwan University (SKKU)
Suwon 16419, Republic of Korea
E-mail: kimjaeyun@skku.edu
The ORCID identification number(s) for the author(s) of this article can be found under https://doi.org/10.1002/adfm.202209874.

DOI: 10.1002/adfm.202209874

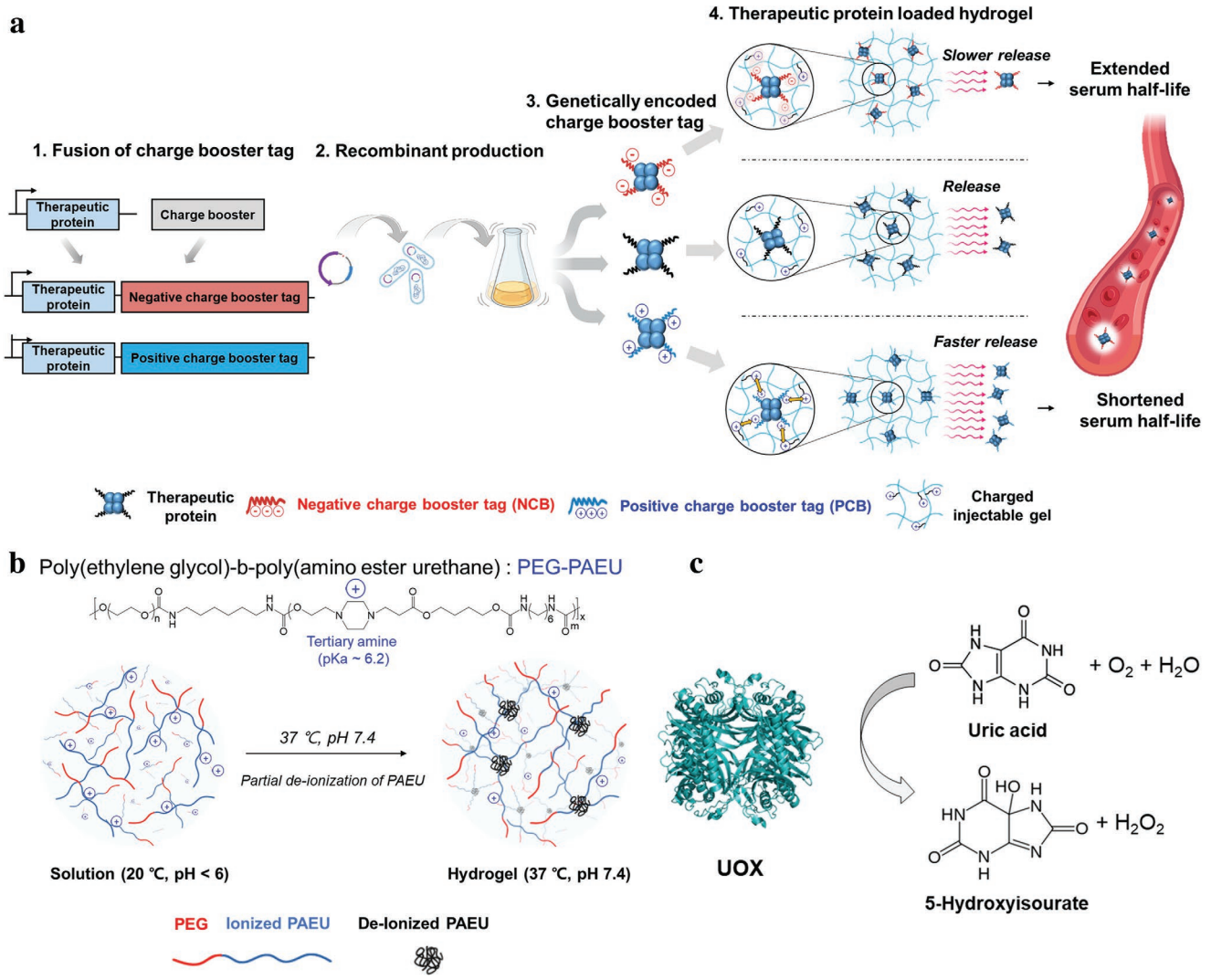

Figure 1. Schematic illustration of a) controlled release of therapeutic proteins from cationic hydrogels by introducing a charge booster tag and b) phase transition of the injectable hydrogel PEG-PAEU depending on the pH and temperature. c) Enzymatic reaction of urate oxidase (UOX), which degrades uric acid.

proteins by introducing a genetically encoded highly charged protein segment (charge booster tag) to the proteins to ultimately regulate their release in the body and enhance their serum half-life, regardless of the intrinsic net charge of the proteins (**Figure 1**a). First, the genes of therapeutic protein variants with a charge booster tag can be prepared using standard cloning techniques. Second, the genes of the therapeutic protein variants can be expressed in host cells, followed by protein purification. Finally, the purified therapeutic protein variants with varying net charges can be mixed with polymers to form an injectable gel for in vitro and in vivo characterization. We hypothesized that introducing a booster tag with a negative charge (negative-charge booster tag, NCB) opposite to the charge of the injectable gel could reinforce the electrostatic interactions between the therapeutic protein and gel (Figure S1, Supporting Information), leading to slower release and a prolonged serum half-life of the protein. In contrast, the introduction of a positive-charge booster tag (PCB) was predicted to accelerate the release and shorten the serum half-life of the therapeutic protein.

As a model injectable hydrogel, we used a pH- and temperature-sensitive poly(ethylene glycol)-poly(*β*-amino ester urethane) (PEG-PAEU) hydrogel. This hydrogel has a positive charge and exhibits a solution state at low pH and room temperature (approximately pH 6 and 25 °C) because of the hydrophilicity of PEG and repulsion of positively charged PAEU.[23,24] When the pH and temperature increase to match the physiological conditions in the human body (pH 7.4 and 37 °C), PEG-PAEU is partially deionized, and a stable hydrogel is formed via hydrophobic interactions (Figure 1b). As a model therapeutic protein, we chose urate oxidase (UOX), which is used to treat gout.[25] UOX catalyzes the conversion of insoluble uric acid to a soluble metabolite (5-hydroxyisourate), lowering the serum concentration of uric acid (Figure 1c). UOX is a homo-tetramer and has a net negative charge under physiological conditions. We investigated whether the introduction of a negatively- or

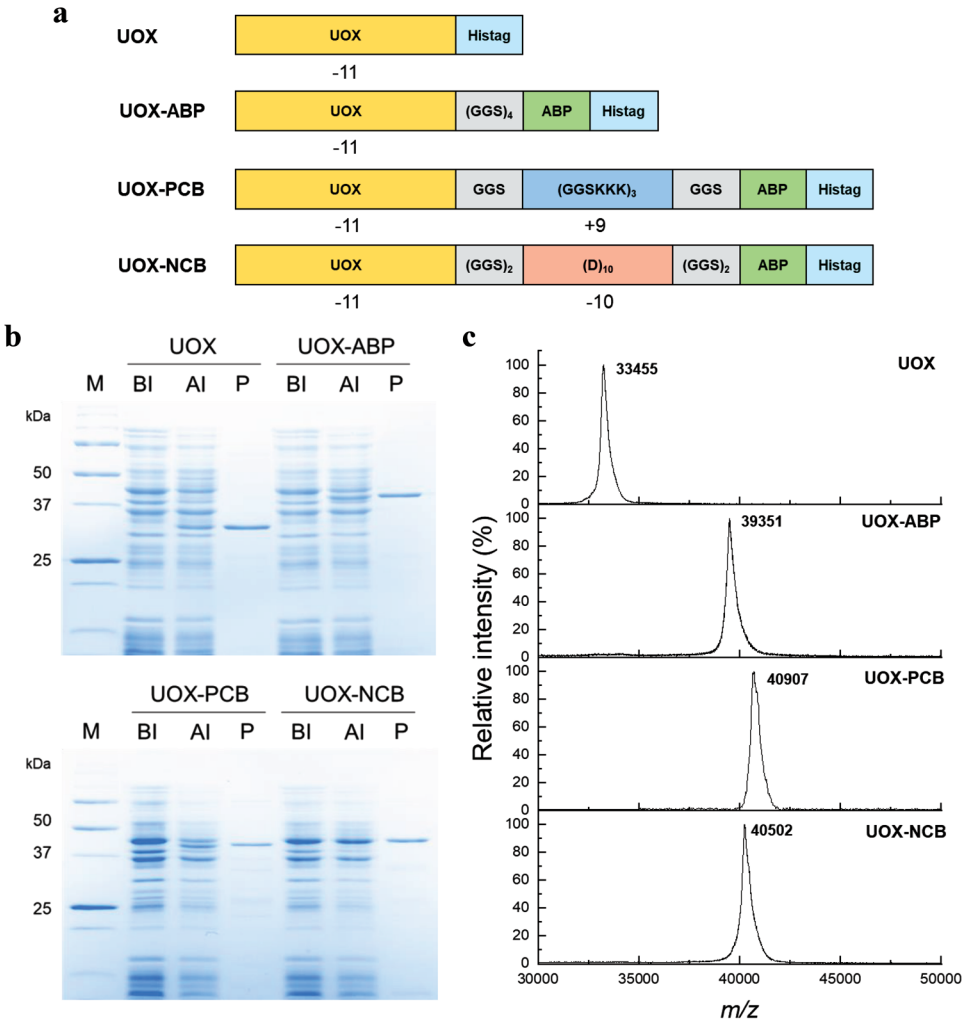

Figure 2. Design and characterization of UOX variants. a) Schematic representation of the structures of the UOX variants. Net charges of UOX, PCB, and NCB are shown below. b) Coomassie brilliant blue-stained protein gels. Lane M, molecular weight standards; BI, before induction; AI, after induction; P, purified protein. c) Mass spectra of UOX variants obtained using MALDI-TOF mass spectrometry analysis.

positively-charged protein segment affected the in vitro release of UOX from the positively charged PEG-PAEU gel, as well as altered the serum half-life.

2. Results and Discussion

2.1. Design of Charge Booster Segments and UOX Variants

We used albumin affibody (ABP)-fused UOX (UOX-ABP) as well as unmodified UOX as therapeutic proteins. ABP is a short peptide derived from *Streptococcus* protein G and has a very high binding affinity (femtomolar dissociation constant) to albumin;[26] thus, albumin is expected to extend the serum half-life of UOX-ABP through neonatal Fc receptor (FcRn)-mediated recycling.[27] Therefore, we generated UOX-ABP using a flexible $(GGS)_4$ fusion linker (**Figure 2**a). We then designed two types of charge-boosting protein segments (Figure 2a). To minimize unwanted intramolecular electrostatic interactions, we used only one type of charged amino acid in each booster tag. As an NCB, we designed a short peptide of 22 residues containing 10 aspartic acids, which was predicted to reduce release from the PEG-PAEU hydrogel by increasing attractive electrostatic interactions. Next, we designed another short peptide of 27 residues containing nine positively charged lysine residues as the PCB to increase the repulsive electrostatic interactions and accelerate protein release from the hydrogel. The charge booster peptide was introduced to the $(GGS)_4$ region of UOX-ABP, which was distant from the catalytic site or oligomer formation interfaces of UOX. A total of three UOX variants were prepared: UOX-ABP (net −36 charge), UOX variant containing PCB and ABP (UOX-PCB, net 0 charge), and UOX variant containing NCB and ABP (UOX-NCB, net −76 charge) (Figure 2a; Table S1, Supporting Information).

2.2. Preparation and Characterization of UOX Variants

Preparation of *Escherichia coli* transformant cells harboring the plasmid encoding each UOX variant and the expression of each

variant are described in the Experimental Section. Using bacterial cell pellets expressing each UOX variant, we purified the designed variants through affinity-based chromatography using a hexahistidine tag and a nickel-charged NTA agarose resin and analyzed the obtained proteins using sodium dodecyl sulfate-polyacrylamide gel electrophoresis (Figure 2b). Overall, the detected bands corresponded to the expected molecular weights of UOX (33.4 kDa), UOX-ABP (39.3 kDa), UOX-NCB (40.9 kDa), and UOX-PCB (40.5 kDa); the UOX variants showed high purity (>90%). Further analysis of these proteins by matrix-assisted laser desorption ionization/time-of-flight (MALDI-TOF) mass spectrometry showed that the intact masses of UOX, UOX-ABP, UOX-PCB, and UOX-NCB were 33252, 39483, 40716, and 40262 m z^{-1}, respectively, which agreed well with the expected intact masses (33455, 39351, 40907, and 40502 m z^{-1}, respectively) with a deviation of less than 1% (Figure 2c). Hence, the designed UOX variants were successfully expressed and purified. Next, analysis of the enzymatic activity of the designed UOX variants showed that the variation in their enzymatic activity was not significant ($p > 0.05$) (Figure S2, Supporting Information). This result implies that charge booster tags do not reduce the efficacy of the UOX in vitro.

2.3. Characterization of PEG-PAEU

The PEG-PAEU hydrogel was synthesized as previously reported[28] (Figure S3a, Supporting Information) and its average molecular weight was verified using gel permeation chromatography (Figure S3b, Supporting Information). The synthesized PEG-PAEU (number average molecular weight: 8021) had a higher molecular weight than that of PEG (number average molecular weight: 2050), which is attributed to the backbone of the synthesized copolymer. In addition, the chemical structure of the synthesized PEG-PAEU was confirmed by nuclear magnetic resonance analysis, indicating the sucessful polymerization (Figure S3c, Supporting Information). The titration curve of the obtained PEG-PAEU revealed that its pKa value was 6.2 (Figure S3d, Supporting Information); thus, the pH sensitivity of the synthesized copolymer is suitable for encapsulating therapeutic agents and using them for use in the biomedical field. Based on these results, its sol–gel transition was determined using the vial tilting method. The sol–gel phase diagram showed that when the pH of the hydrogel solution was lower than pH 6.0, the sol did not form a gel, even when the temperature was increased. In turn, the sol formed a hydrogel under physiological conditions of 37 °C and pH 7.4 (**Figure 3**a,b). PEG-PAEU exists in the sol state because the tertiary amine group in the PAEU chain is ionized and the resulting copolymer is hydrophilic. Therefore, when the pH and temperature increase, the tertiary amine begins to deionize, and hydrophobic interactions between the deionized PAEU chains result in physical crosslinking, forming the gel state of the copolymer.

The mechanical properties of PEG-PAEU were investigated via rheological analysis (Figure S3e, Supporting Information). The storage modulus (G′) of PEG-PAEU at the injection point (pH 6.0) was lower than its loss modulus (G″), indicating that the hydrogel solution was in the sol state and could be injected. In contrast, G′ was higher than G″ under body conditions (pH 7.4), indicating the formation of a hydrogel. The mechanical properties of PEG-PAEU mixed with uricase variants (28 μM) at two different pH conditions (6.2, 7.4) were investigated via rheological analysis (Figure S4, Supporting Information). The rheological analysis was conducted under conditions of PAEU hydrogel being loaded with UOX variants because the charge change of hydrogel due to interaction between PAEU hydrogel and various charges of UOX variants can affect the mechanical property of hydrogel. The storage modulus (G′) of PEG-PAEU loaded with all types of uricase variants at the injection point (pH 6.2) was lower than its loss modulus (G″), indicating that the hydrogel solution was in the sol state and could be injected. In contrast, G′ was higher than G″ under body conditions (pH 7.4) regardless of type of uricase loaded, indicating the formation of a hydrogel. The rheological data represents that the type of uricase at the concentration that we used throughout the studies did not affect the gel injectability.

The swelling rate of PEG-PAEU was observed by measuring the weight change of the hydrogel immersed in water (Figure S5, Supporting Information). The swelling ratio of PEG-PAEU was 3.93 which was calculated by substituting the weight after swelling and drying. The PEG-PAEU hydrogel showed a degradation property in physiological conditions

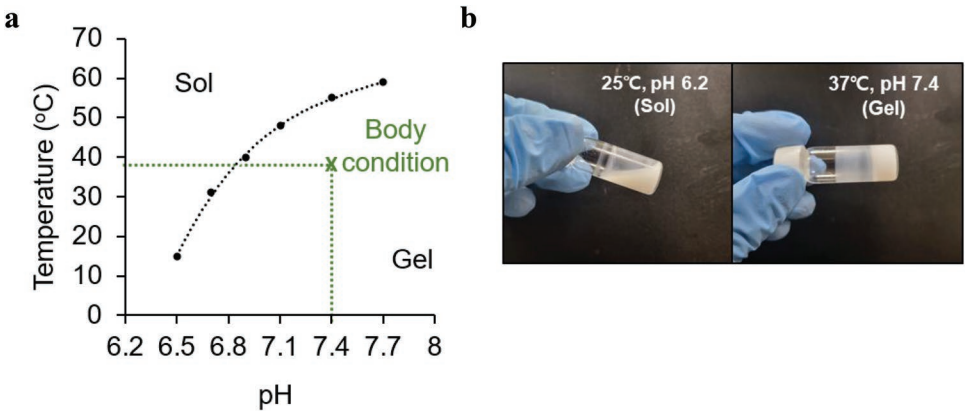

Figure 3. pH- and temperature-sensitive phase transition of PEG-PAEU hydrogels. a) In vitro sol–gel phase diagram of PEG-PAEU in relation to pH and temperature. b) In vitro sol–gel phase transition of PEG-PAEU at different pH and temperatures.

such as PBS and DMEM containing FBS at 37 °C (Figure S6, Supporting Information). More than half of PEG-PAEU still remained after 2 weeks which shows that PEG-PAEU is suitable UOX carrier for long-term treatment. In addition, PEG-PAEU exhibited high biocompatibility based on the viability of L929 cells in the presence of increasing concentrations of PEG-PAEU observed by MTT assay (Figure S7, Supporting Information) and live/dead fluorescent assay (Figure S8, Supporting Information). L929 fibroblast cells are selected for in vitro cytotoxicity test because fibroblast is one of the major cell types of subcutaneous region where PEG-PAEU is supposed to be placed after s.c. injection. In summary, PEG-PAEU was biocompatible, showed good injectability, and formed a gel and maintained its form after being introduced into the body.

2.4. In Vitro Release of UOX Variants from PEG-PAEU

To investigate the in vitro release of UOX from the PEG-PAEU hydrogel, we monitored the amount of each UOX variant released at different time points. Each UOX variant was mixed with PEG-PAEU in solution, and the pH and temperature were adjusted to pH 7.4 and 37 °C, respectively. After PEG-PAEU formed a hydrogel, the release of each UOX variant was monitored for 7 days (**Figure 4**). As expected, UOX release was related to the net charge of the protein. Over 7 days, 56% and 59% of UOX with an intrinsic negative charge (net –44 charge) and UOX-ABP (net –36 charge) were released (Figure 4). Additionally, 76% of neutral UOX-PCB (net 0 charge) was released, indicating faster release compared to unmodified UOX. In contrast, only 51% of UOX-NCB (net –76 charge) was released from the hydrogel over 7 days. These results show a faster release trend as the net negative charge of the UOX variant decreased. We also investigated the effect of the charge booster tag on the diffusion of the UOX variant inside the hydrogel using Fick's second law[29] (Figure 4). The diffusion coefficient of the UOX variants was related to the net charge of UOX, similar to the release rate. For example, UOX-PCB showed a 183% higher diffusion coefficient than unmodified UOX, whereas that of UOX-NCB was 86%. As the net positive charge of PEG-PAEU hydrogel was constant across groups, different types of charge booster tags enhanced or reduced the interactions between UOX and the PEG-PAEU hydrogel.

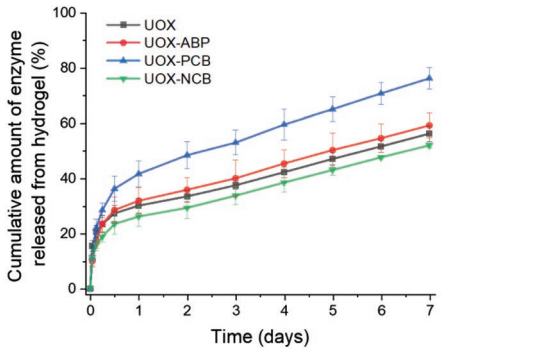

	UOX	UOX-ABP	UOX-PCB	UOX-NCB
Diffusion coefficient (10^{-3}, cm^2/day)	0.36 ± 0.04	0.40 ± 0.06	0.65 ± 0.07	0.30 ± 0.01

Figure 4. In vitro release of UOX variants from the PEG-PAEU hydrogel. Release profile of UOX variants over 1 week and diffusion coefficient of UOX variants from the hydrogels.

2.5. In Vivo Half-Life of UOX Variants with Different Charges

We investigated the pharmacokinetics of UOX variants without PEG-PAEU to assess whether the charge booster tag or ABP prolonged the serum half-life of UOX (**Figure 5**a). When the UOX variants were directly (without hydrogel) injected subcutaneously into mice, all variants exhibited an initial burst of release for 6 h, followed by rapid removal. The half-life of unmodified UOX was 3.3 h, whereas those of UOX-ABP, UOX-PCB, and UOX-NCB were 16.0, 15.7, and 14.5 h, respectively (Figure 5a). In the case of UOX, 90% of serum activity was eliminated at 12 h, with maximum activity at 6 h, suggesting rapid UOX diffusion into the blood followed by rapid removal from the body fluids through renal filtration. However, when ABP was fused with UOX, all groups were eliminated more slowly compared to unmodified UOX after the fast initial burst. Indeed, more than 4 days were required for ABP-fused UOX variants to reach 10% of the maximum serum activity, suggesting that subcutaneously injected ABP-fused UOX remains in the body for a long time, likely because of the FcRn-mediated recycling of albumin.[5,27] Nevertheless, ABP fused to each UOX variant may have had different albumin-binding affinities. To investigate this prediction, we measured the amount of the UOX-ABP variant bound to albumin. Considering that the half-maximal binding concentrations of each ABP-fused UOX variant were similar in scale (nM), the binding ability of ABP was maintained even after fusion to UOX (Figure S9, Supporting Information). Furthermore, the release profile of UOX fused with different charge booster tags was independent of their charge. Hence, modifying the electrostatic interaction through a charge booster tag did not extend the half-life when the protein was administered without an antagonistically charged hydrogel.

2.6. In Vivo Half-Life of Charged UOX Delivered by Injectable Hydrogel

Next, we investigated the pharmacokinetics of charged UOX carried by PEG-PAEU to assess whether the modulated electrostatic interactions between the UOX variants and hydrogel affect the sustained release of the protein according to different charge booster tags (Figure 5; Figure S11, Supporting Information). The UOX variants with PEG-PAEU hydrogel exhibited an initial burst, but the maximum serum activity was observed at a later time compared with that of UOX variants without PEG-PAEU (Figure 5a). These results show that the PEG-PAEU hydrogel can delay the rapid dilution of the therapeutic proteins from tissues to the blood. Coadministration of UOX and PEG-PAEU increased the serum half-life of UOX from 3.3 to 49.3 h, likely because of sustained release from the hydrogel. For UOX variants, the serum half-life increased with hydrogel-induced sustained release, as well as proportionally with enhanced electrostatic interactions, with the serum half-lives of

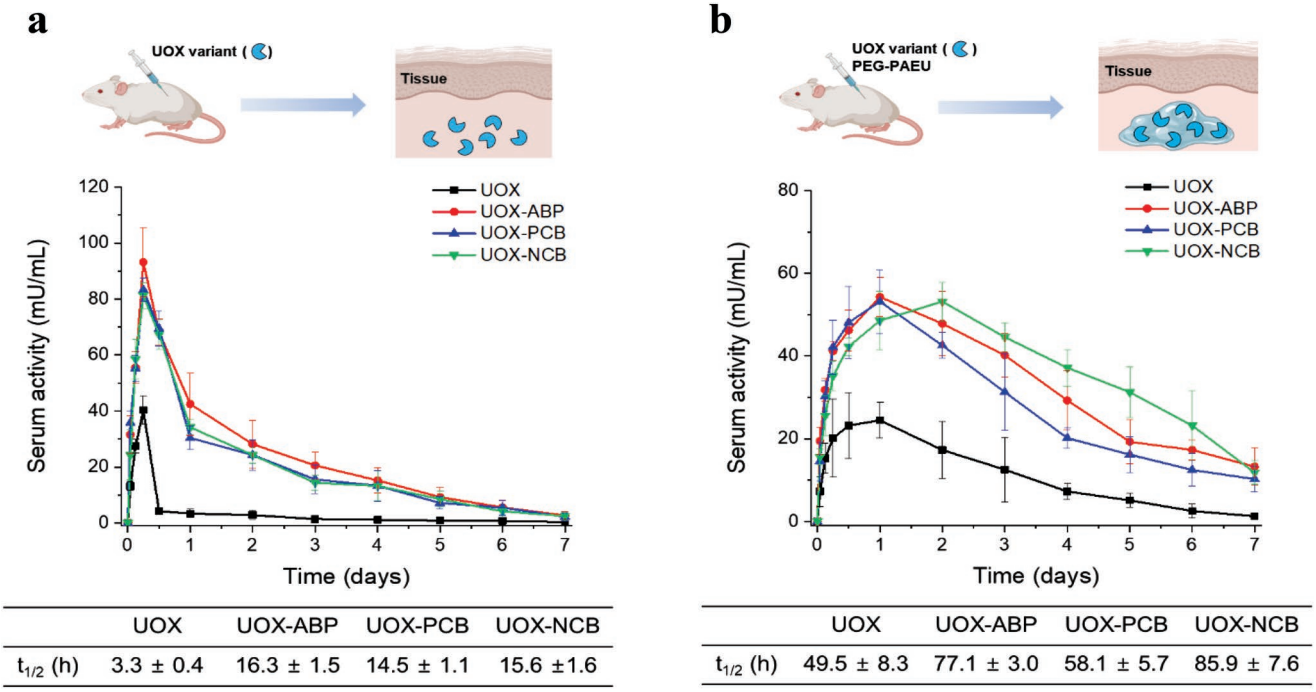

	UOX	UOX-ABP	UOX-PCB	UOX-NCB
$t_{1/2}$ (h)	3.3 ± 0.4	16.3 ± 1.5	14.5 ± 1.1	15.6 ±1.6

	UOX	UOX-ABP	UOX-PCB	UOX-NCB
$t_{1/2}$ (h)	49.5 ± 8.3	77.1 ± 3.0	58.1 ± 5.7	85.9 ± 7.6

Figure 5. Pharmacokinetics of UOX variants subcutaneously administrated a) alone or b) in combination with PEG-PAEU injectable hydrogel.

UOX-PCB, UOX-ABP, and UOX-NCB increasing to 58.1, 77.1, and 85.8 h, respectively. Thus, the degree of net negative charge of the UOX variant positively correlates with the serum half-life of the UOX variants (Figure 5b). Although UOX-PCB had a lower net negative charge compared to UOX, the half-life was improved through FcRn-mediated recycling, as observed previously when UOX variants were administrated without hydrogel. Consequently, sustained release of the therapeutic protein from the hydrogel is dependent on the type of charge booster tag modification applied.

2.7. In Vivo Half-Life of Charged UOX Delivered by Injectable Hydrogel in the Presence of Human Serum Albumin

Finally, we further investigated the relationship between the net charge of the therapeutic protein and its serum half-life by exploring its albumin-binding capacity. Therefore, we added a net negative charge to the UOX variants by adding human serum albumin (HSA; net –15 charge) before mixing the variants with PEG-PAEU (**Figure 6**a). Due to very high affinity of ABP to HSA (K_d ≈50 fM),[26] we expected the majority of HSA added binds ABP. Coadministration of HSA further increased the half-lives of UOX-PCB, UOX-ABP, and UOX-NCB to 77.2, 96.2, and 106.1 h respectively (Figure S10, Supporting Information). Considering that an identical net negative charge was added to the UOX variants, these results demonstrate that modulating the net charge can effectively regulate the sustained release of therapeutic proteins from hydrogels. When we plotted the serum half-life versus net charge of the UOX variants, a strong negative correlation ($R^2 = 0.966$) was observed (Figure 6b). These results suggest that using a charge booster tag to modulate the net charge can modify the half-life of therapeutic protein as necessary.

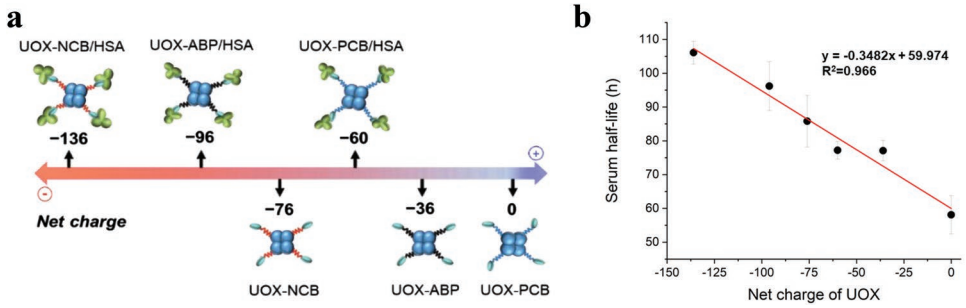

Figure 6. Effect of net charge on the serum half-life of charge booster tag-fused UOX. a) Schematic illustration of UOX variants with different net charges. b) Correlation between the serum half-life and net charge of UOX variants subcutaneously injected with PEG-PAEU hydrogel.

2.8. In Vivo Uric Acid-Lowering Efficacy of the UOX Variants Loaded in PEG-PAEU

In the previous research, the serum activity greater than 10 mU mL^{-1} of UOX was effective in treating hyperuricemia in mice models.[24] In Figure 5 and Figure S6 (Supporting Information), the serum activities of UOX-NCB and UOX-NCB/HSA were maintained above 10 mU mL^{-1} between days 1 and 7. Therefore, we believe that the serum activity above 10 mU mL^{-1} is suitable to evaluate the efficacy of UOX samples released from the hydrogel. Based on this, we evaluated the in vivo efficacy of UOX samples on day 4.

We chose three representative UOX samples with or without a charge booster tag (UOX-PCB, UOX-ABP, and UOX-NCB/HSA) loaded in PEG-PAEU hydrogel. For comparison, we also chose the free UOX sample. Considering the long serum half-lives of the three UOX samples loaded in PEG-PAEU hydrogel (58 to 106 h), we induced hyperuricemia in mice at 96 h after the injection of the UOX samples. All three UOX samples loaded in PEG-PAEU hydrogel showed the substantial uric acid-lowering efficacy, which was greater than that of free UOX sample (**Figure 7**). At three time points (1, 3, and 6 h after hyperuricemia induction), the uric acid-lowering efficacy was in the increasing order of UOX-PCB, UOX-ABP, and UOX-NCB/HSA, which matches well with the order of serum half-life of the samples. Even at 12 h after hyperuricemia induction, UOX-NCB/HSA exhibited the significantly greater uric acid-lowering efficacy than UOX-PCB. Overall, these findings demonstrated that the favorable electrostatic interactions between UOX variants and PEG-PAEU enables the sustained release of UOX variant from the hydrogel, according to the net negative charge of UOX variants, and so the uric acid-lowering efficacy of the UOX samples was maintained for multiple days.

The rapeutic proteins typically show a limited serum half-life. To overcome this limitation, hydrogels are often used for the sustained release of therapeutic proteins. Despite efforts aimed at improving the electrostatic interactions between therapeutic proteins and hydrogels to increase the serum half-life of proteins, this approach is not effective for weakly charged therapeutic proteins. Therefore, we designed a cationic/anionic peptide to act as a charge booster tag that can be fused to therapeutic proteins to regulate their serum half-life and enhance their interactions with hydrogels.

Herein, we used UOX as a therapeutic protein model and modified it based on the hypothesis that modulation of its charge is highly related to its sustained release from hydrogels. When the net negative charge was decreased or increased by fusing UOX with PCB or NCB, respectively, its release from the PEG-PAEU hydrogel was consistent with the magnitude of the protein net charge. Our designed PCB, which had a positive charge, induced faster release of the protein from the hydrogel, whereas the presence of NCB reduced the release rate, which is better suited for the administration of therapeutic proteins. Furthermore, our strategy may reduce the loss of functionality of therapeutic proteins and ABP and enhance the serum half-life through FcRn-mediated recycling in the blood.

In summary, we developed a charge booster tag system for the controllable release of therapeutic proteins from hydrogels. Our designed charge booster tags may be useful for controlling the half-life of weakly charged protein by introducing additional

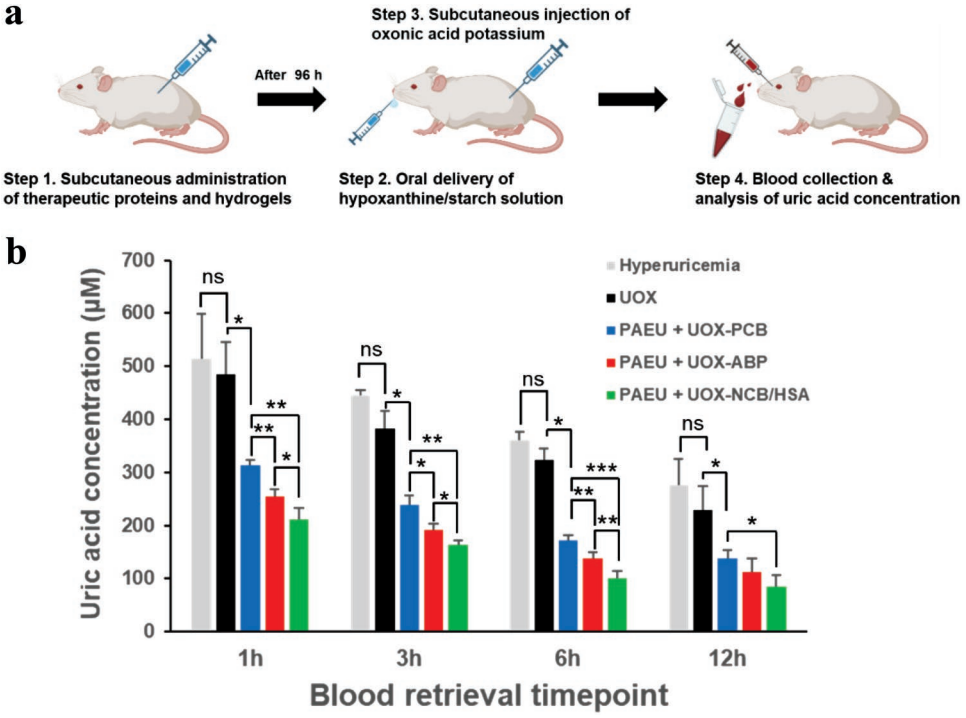

Figure 7. In vivo uric acid lowering effect of UOX variants. a) Experimental scheme of preparing hyperuricemia model and collection of blood samples. b) Uric acid concentration in the mice treated with UOX without PEG-PAEU and UOX-PCB, UOX-ABP, and UOX-NCB/HSA loaded with PEG-PAEU. The data are represented as mean ± SD and were subjected to one-way ANOVA with Tukey's post-hoc test. *$p < 0.05$, **$p < 0.01$, ***$p < 0.001$.

charges and thus improving electrostatic interactions between the therapeutic protein and vehicle hydrogels. By using the charge booster tag system, we extended the half-life of UOX compared with that of unmodified UOX. Given that each therapeutic protein has different intrinsic charge states, our proposed strategy can be used as a general platform for the controlled release of various therapeutic proteins from hydrogels.

3. Experimental Section

Materials: Nitrilotriacetic acid agarose beads were purchased from Qiagen (Hilden, Germany). PD-10 desalting columns were purchased from GE Healthcare (Chicago, IL, USA). Isopropyl-β-D-thiogalactopyranoside (IPTG) was purchased from Thermo Fisher Scientific (Waltham, MA, USA). Vivaspin 6 concentrator (MWCO: 10000 Da) was purchased from Sartorius (Göttingen, Germany). The rabbit anti-his tag antibody and horseradish peroxidase-conjugated anti-rabbit IgG were purchased from Cell Signaling Technology (Danvers, MA, USA). Yeast extract, tryptone, and agar were obtained from DB Biosciences (San Jose, CA, USA). *Bsi*WI and *Hind*III were purchased from New England Biolabs (Ipswich, MA, USA). All other reagents were purchased from Sigma-Aldrich (St. Louis, MO, USA) unless otherwise specified. All reagents were of analytical grade and used without further purification.

Plasmid Construction: To construct the plasmid expressing UOX, its encoding gene was synthesized by Macrogen (Seoul, Korea) and cloned into a pQE80 vector to generate pQE80-UOX. To generate ABP-fused UOX, the genes encoding each linker and ABP were synthesized by Macrogen and subcloned into pQE80-UOX using the restriction enzymes *Bsi*WI and *Hind*III.

Expression and Purification: To express the UOX variants, the authors transformed each plasmid (pQE80-UOX, pQE80-UOX-ABP, and pQE80-UOX-NCB) into chemically competent TOP10 *Escherichia coli* cells. For PCB-fused UOX, the pQE80-UOX-PCB plasmid was transformed into chemically competent BL21(DE3) cells. Transformed cells were plated onto agar plates containing 100 μg mL^{-1} of ampicillin and incubated at 37 °C for 14 h. A single colony was inoculated into fresh 2xYT medium and incubated at 37 °C overnight for pre-culture. The transformed cells (2 mL) were inoculated into 200 mL fresh 2xYT media (1:100, v v^{-1}%) with 100 μg mL^{-1} ampicillin and incubated at 37 °C with 200 rpm agitation. When the optical density at 600 nm reached 0.6, 1 mM of IPTG was added, and the culture was incubated at 18 °C for additional 18 h. For cationic UOX, transformed cells were incubated at 18 °C for 6 h after adding IPTG. After incubation, the cultured cells were harvested by centrifugation at 4000 × *g* for 10 min. Harvested cells were stored at −80 °C until use. To purify the UOX variants, the authors conducted immobilized metal affinity chromatography as previously reported.[4] Purified UOX was analyzed using sodium dodecyl sulfate-polyacrylamide gel electrophoresis, and the protein concentration was measured at 280 nm. The molar extinction coefficient of the UOX variants was 33 920 cm^{-1} M^{-1} (UOX) and 36 900 cm^{-1} M^{-1} (UOX-ABP, UOX-PCB, and UOX-NCB) as determined by the equation $\varepsilon 280 = (5500 \times n_{\text{Triptophan}}) + (1490 \times n_{\text{Tyrosine}}) + (125 \times n_{\text{Disulfide bond}})$.

MALDI-TOF Mass Spectrometry Analysis: The purified UOX variants were solvent-exchanged with 0.1% trifluoroacetic acid using Zebaspein (MWCO: 7 KDa) according to the manufacturer's protocol (Thermo Fisher Scientific). UOX variants were mixed with an equal volume of sinapic acid-saturated acetonitrile with trifluoroacetic acid solution (0.1%) in a 3:7 ratio. UOX samples were subjected to a sinapic acid layer prepared using a sinapic acid-saturated ethanol solution. The mass spectra were obtained using Autoflex MALDI-TOF (Bruker, Billerica, MA, USA) and analyzed using flexAnalysis v3.4 software (Bruker). Calibration was conducted using protein standard II (20–90 kDa) before the measurement.

Enzymatic Activity of UOX Variants: To investigate whether charge booster tags affect the enzymatic activity of UOX, the authors compared uric acid degradation as described previously with slight modifications.[24] UOX variants (10 nM) were briefly reacted with 200 μM uric acid for 10 min in in PBS buffer (pH 7.4). The degradation of uric acid was measured by monitoring changes in absorbance at 293 nm.

In Vitro Albumin Binding Assay: HSA was dissolved in phosphate-buffered saline (PBS, pH 7.4) at 100 μg mL^{-1}, and 100 μL HSA was added to an immunoplate (SPL Life Sciences, Pocheon, Korea). The plate was incubated overnight at 4 °C for passive adsorption of HSA. After incubation, the wells were washed three times using PBS-T solution (0.05% Tween 20 in PBS buffer), and 5% skim milk in PBS-T was added at room temperature for 2 h to prevent non-specific adsorption. Various concentrations of the UOX variants (0.01–1000 nM) were prepared using 5% skim milk in PBS-T and added at room temperature for 1 h. Each well was washed three times with PBS-T and an anti-his tag rabbit antibody (diluted 1:1000 in 5% skim milk [v v^{-1}%]) was added and incubated at 23 °C for 1 h. The plate was washed three times with PBS-T, and anti-rabbit horseradish peroxidase-conjugated antibody (diluted 1:3000 [v v^{-1}%] in 5% skim milk) was added and incubated at room temperature for 1 h. Next, 100 μL of 3,3′,5,5′-tetramethylbenzidine was added to each well, and the reaction was quenched using 2 M H_2SO_4 for 5 min. Absorbance at 450 nm was measured, and the graph was fitted using OriginPro 2019 software (OriginLab, Northampton, MA, USA).

Synthesis of PEG-PAEU: Multiblock copolymer PEG-PAEU was synthesized via a two-step reaction in accordance with a previous report.[28] First, HPB monomer was synthesized by a Michael addition reaction between 1-(2-hydroxyethyl)piperazine and 4-hydroxylbutyl acrylate. Next, PEG-PAEU was synthesized via poly-addition reaction between the dihydroxyl group from PEG and the HPB monomer, as well as the diisocyanate group from HDI. Dibutyltin dilaurate was added to act as a catalyst during synthesis.

Characterization of PEG-PAEU: The average molecular weights of PEG and PEG-PAEU were measured by gel permeation chromatography using an Agilent 1260 Infinity system with a refractive index detector (Agilent RI-1260; Agilent Technologies, Santa Clara, CA, USA). N,N-Dimethylformamide was used to dissolve PEG-PAEU (10 mg mL^{-1}), and polystyrene standards (Polymer Standard Service GmbH, Mainz, Germany) were used to calibrate the equipment.

The chemical structure of the synthesized multiblock copolymer PEG-PAEU was detected with a ^{1}H nuclear magnetic resonance measurement using Unity Inova 500 MHz Spectrometer (Varian Medical Systems, Palo Alto, CA, USA). The samples were dissolved in $CDCl_3$ solvent for analysis.

The pKa value of PEG-PAEU was determined using the acid-base titration method, in which 40 mg of the copolymer was dissolved in 40 mL of distilled water. The pH was increased from 3.0 to 11.0 by adding 0.1N NaOH in a dropwise manner. The titration curve was drawn by measuring the pH value immediately after NaOH was added. The pKa value was determined as the inflection point of the titration curve.

A sol–gel phase diagram was obtained by first preparing six samples of 20 wt.% hydrogel solution in a 5 mL vial by suspending the copolymer in PBS solution at room temperature. The pH of each sample was adjusted to six different conditions by adding 5N HCl or 5N NaOH. Vials with hydrogel solution were stabilized overnight at 4 °C. For analysis, the vials were placed in a water bath, and the temperature was increased starting at 10 °C. The samples were subjected to a 15 min equilibration period each time the temperature was raised by 2 °C. The diagram was drawn by recording the temperature when the phase transition occurred. The sol–gel transition of PEG-PAEU was also investigated using the vial-tilting method using 1 mL of 20 wt.% hydrogel solution prepared under two different pH and temperature conditions.

The storage modulus (G') and loss modulus (G') of the hydrogel solution were measured under two different pH conditions (pH 6.0 and 7.4), increasing the temperature to investigate the mechanical properties under each condition. The shear stress and frequency used in the measurement were set to 0.4 Pa and 1 rad s^{-1}, respectively. The temperature was measured from 10 to 40 °C. The heating rate was 1 °C min^{-1}.

Swelling Test of PEG-PAEU Hydrogel in Water: PEG-PAEU hydrogel right after gelation was immersed in water and the weight of hydrogel was measured at designated time points up to 24 h. The weight of swollen hydrogel was compared to the weight of hydrogel before immersed in water.

Biodegradability Test of PEG-PAEU Hydrogel: The degradation of PEG-PAEU hydrogel was investigated by measuring the remaining weight of PEG-PAEU in PBS and DMEM containing 10% FBS, respectively. PEG-PAEU solution (200 µL) (20 wt.%, pH 6.2) was subcutaneously injected into the C57BL/6 mouse to form PEG-PAEU hydrogel. The PEG-PAEU hydrogel was retrieved from the animal 1 h after the injection and immersed in PBS or DMEM containing 10% FBS at 37 °C. The immersed PEG-PAEU hydrogel was retrieved from the media at predetermined time points (1, 3, 5, 7, and 14 days) and subsequently freeze-dried. The weight of freeze-dried hydrogel was compared with the original freeze-dried weight of initial hydrogel.

In Vitro Cytotoxicity Test: L929 cells were seeded into 96-well plates containing Dulbecco's modified Eagle's medium (Gibco, Grand Island, NY, USA) and incubated for 1 day. Different concentrations of PEG-PAEU copolymer (10–1000 µg mL^{-1}) were added to each well and incubated for 1 day. MTT solution (20 µL) was added to each well and incubated for 3 h, after which the medium was removed and the cells were resuspended in 200 µL of fresh medium and incubated for an additional hour. The absorbance at 490 nm was measured using a microplate reader. Cells in fresh medium without copolymer were used as a reference (100% cell viability). Live/dead fluorescent assay was also conducted by staining live cells with Calcein AM in green and dead cells with ethidium homodimer (EthD-1) in red. After staining, live and dead cells were observed by inverted fluorescence microscope at excitation wavelengths of 490 and 530 nm, respectively.

In Vitro UOX Release Study: A 200-mg hydrogel solution (20 wt.%) was prepared by mixing lyophilized PEG-PAEU with four UOX variants (28 µM): i) unmodified UOX, ii) UOX-ABP, iii) UOX-NCB, and iv) UOX-PCB. The mixed solution was stabilized overnight at 4 °C, and the pH of the resulting solution was adjusted to 7.4. The mixture was incubated at 37 °C for 4 h to form PEG-PAEU hydrogel-encapsulating UOX. PBS (1 mL) was then added as a supernatant on the hydrogel surface in the multi-well plate. At the designated time point, 1 mL of supernatant was collected and replaced with 1 mL of fresh PBS at 37 °C. The enzymatic activity of the UOX variants released in the supernatant was measured at each time point in a uric acid assay. Briefly, the supernatant containing the released UOX was mixed with a uric acid solution (200 µM), and the uric acid degradation rate was calculated by monitoring changes in absorbance at 293 nm. The diffusion coefficient (D) was obtained using Fick's second law according to the equation $\frac{M_t}{M_\infty} = 2\left(\frac{Dt}{\pi d^2}\right)^{1/2}$, where M_t and M_∞ denote the total amount of protein released during the time period t and after infinite time, respectively, and d represents half of the thickness of PEG-PAEU.[29]

In Vivo UOX Release Study: All animal experimental procedures were approved by the Institutional Animal Care and Use Committee of Sungkyunkwan University (No. SKKUIACUC2020-06-34-1). Eight-week-old female C57BL/6 mice ($n = 4$) were used for the in vivo release test. Four UOX variants (unmodified UOX, UOX-ABP, UOX-PCB, and UOX-NCB) were prepared in two forms (free and hydrogel-encapsulated) with concentration of 28 µM. Additionally, the three UOX variants (UOX-ABP, UOX-PCB, and UOX-NCB) were mixed with HSA and then applied to PEG-PAEU. The UOX-mixed PEG-PAEU hydrogel precursor solution was prepared by mixing PEG-PAEU (20 wt.%) with the UOX variants at pH 6.2 followed by incubation for 4 h at room temperature. The samples were subcutaneously injected into the flank of the mice. The blood samples were collected at designated time points (1, 3, 6, 12 h, 1, 2, 3, 4, 5, 6, and 7 days) from the retro-orbital plexus after injection. After injection, blood samples were collected from the retro-orbital plexus at designated time points. The serum was separated from the collected blood samples via centrifugation (6,000 × g at 4°C for 15 min) and preserved at 4 °C until analysis. The serum samples were analyzed in a uric acid degradation assay to measure the enzymatic activity of released UOX in the serum.[5]

In Vivo Hyperuricemia Therapeutic Study: Uric acid lowering efficacy of uricase variants was analyzed by treating hyperuricemia-induced mouse model. Hyperuricemia model mouse for the test was prepared by following the previously reported papers.[30] Eight-week-old female C57BL/6 mice ($n = 4$) were used to induce hyperuricemia to investigate the uric acid lowering effect of uricase variants released from PEG-PAEU. Hyperuricemia-induced mice were arranged into 5 groups: i) mice treated with PBS (positive control), ii) mice treated with free UOX, iii) mice treated with UOX-ABP-loaded PEG-PAEU, iv) mice treated with UOX-PCB-loaded PEG-PAEU, v) mice treated with UOX-NCB/HAS-loaded PEG-PAEU. First four types of uricase variants were injected with different formulations to each group of mice. After 96 h, hyperuricemia was induced to mice by oral administration of hypoxanthine dissolved in 3% starch solution and subcutaneous injection of oxonic potassium salt in order. After hyperuricemia was induced, blood samples were collected from mice at designated time points (1, 3, 6, and 12 h). Serum was separated after the blood samples were centrifuged. Undegraded uric acid concentration in serum was analyzed using uric acid assay kit (KA1651, Abnova, Taiwan).

Statistical Analysis: Statistical analysis was conducted by one-way ANOVA for multiple comparisons followed by Tukey post-hoc test using GraphPad Prism software. Statistical significance of all the analyses was set at *$p < 0.05$, ** $p < 0.01$, *** $p < 0.001$, **** $p < 0.0001$, "ns" means there is no significant difference.

Supporting Information

Supporting Information is available from the Wiley Online Library or from the author.

Acknowledgements

S.K. and D.H.K. contribute equally to this work. This research was funded by the National Research Foundation of Korea (NRF), the Ministry of Science, and ICT (Grant No. 2015M3D3A1A01064923, 2021R1A5A1028138, 2020M3A9D3039720, 2022R1A2B5B02002097).

Conflict of Interest

The authors declare no conflict of interest.

Data Availability Statement

The data that support the findings of this study are available from the corresponding authors upon reasonable request.

Keywords

charge booster tags, injectable gels, serum half-life, therapeutic proteins

Received: August 25, 2022
Revised: November 28, 2022
Published online: December 27, 2022

[1] S. Mitragotri, P. A. Burke, R. Langer, *Nat. Rev. Drug Discovery* **2014**, *13*, 655.
[2] M. N. Hasan, Y. H. Hwang, J. M. An, S. M. Shatil Shahriar, S. Cho, Y.-K. Lee, *ACS Appl. Mater. Interfaces* **2020**, *12*, 38925.

[3] C. Fu, Q. Chen, F. Zheng, L. Yang, H. Li, Q. Zhao, X. Wang, L. Wang, Q. Wantg, *Angew. Chem., Int. Ed.* **2019**, *58*, 1392.
[4] S. Kim, M. Kim, S. Jung, K. Kwon, J. Park, S. Kim, I. Kwon, G. Tae, *J. Controlled Release* **2019**, *309*, 181.
[5] S. I. Lim, Y. S. Hahn, I. Kwon, *J. Controlled Release* **2015**, *207*, 93.
[6] A. L. Swain, M. Jaskólski, D. Housset, J. K. Rao, A. Wlodawer, *Proc. Natl. Acad. Sci. USA* **1993**, *90*, 1474.
[7] A. Synakiewicz, T. Stachowicz-Stencel, E. Adamkiewicz-Drozynska, *Expert Opin Investig Drugs* **2014**, *23*, 1517.
[8] L. M. Parra, R. M. Webster, *Nat. Rev. Drug Discovery* **2022**, *21*, 489.
[9] L. DeFrancesco, *Nat. Biotechnol.* **2022**, *40*, 149.
[10] R. E. Kontermann, *Curr. Opin. Biotechnol.* **2011**, *22*, 868.
[11] C. M. L. Lau, G. Jahanmir, Y. Yu, Y. Chau, *J. Controlled Release* **2021**, *335*, 75.
[12] S. Awwad, A. Abubakre, U. Angkawinitwong, P. T. Khaw, S. Brocchini, *Eur. J. Pharm. Sci.* **2019**, *137*, 104993.
[13] S. H. Kim, T. Thambi, V. H. Giang Phan, D. S. Lee, *Carbohydr. Polym.* **2020**, *233*, 115832.
[14] M. H. Turabee, T. Thambi, J. S. Lym, D. S. Lee, *Biomater. Sci.* **2017**, *5*, 837.
[15] C.-C. Lin, K. S. Anseth, *Adv. Funct. Mater.* **2009**, *19*, 2325.
[16] M. M. Martino, P. S. Briquez, A. Ranga, M. P. Lutoff, J. A. Hubbell, *Proc. Natl. Acad. Sci. USA* **2013**, *110*, 4563.
[17] Y. Li, J. Rodrigues, H. Tomás, *Chem. Soc. Rev.* **2012**, *41*, 2193.
[18] B. Jeong, Y. H. Bae, S. W. Kim, *J. Controlled Release* **2000**, *63*, 155.
[19] D. Gyawali, P. Nair, H. K. W. Kim, J. Yang, *Biomater. Sci.* **2013**, *1*, 52.
[20] V. H. G. Phan, T. Thambi, M. S. Gil, D. S. Lee, *Polymer* **2017**, *109*, 38.
[21] D. H. Kim, Y. K. Seo, T. Thambi, G. J. Moon, J. P. Son, G. Li, J. H. Park, J. H. Lee, H. H. Kim, D. S. Lee, O. Y. Bang, *Biomaterials* **2015**, *61*, 115.
[22] M. K. Nguyen, C. T. Huynh, G. H. Gao, J. H. Kim, D. P. Huynh, S. Y. Chae, K. C. Lee, D. S. Lee, *Soft Matter* **2011**, *7*, 2994.
[23] M. S. Gil, J. Cho, T. Thambi, V. H. G. Phan, I. Kwon, D. S. Lee, *J. Controlled Release* **2017**, *267*, 119.
[24] J. Cho, S. H. Kim, B. Yang, J. M. Jung, I. Kwon, D. S. Lee, *J. Controlled Release* **2020**, *324*, 532.
[25] A. C. Nyborg, C. Ward, A. Zacco, B. Chacko, L. Grinberg, J. C. Geoghegan, R. Bean, M. Wendeler, F. Bartnik, E. O'Connor, F. Gruia, V. Iyer, H. Feng, V. Roy, M. Berge, J. N. Miner, D. M. Wilson, D. Zhou, S. Nicholson, C. Wilker, C. Y. Wu, S. Wilson, L. Jermutus, H. Wu, D. A. Owen, J. Osbourn, S. Coats, M. Baca, *PLoS One* **2016**, *11*, 0167935.
[26] A. Jonsson, J. Dogan, N. Herne, L. Abrahmsén, P.- Å. Nygren, *Protein Eng Des Sel* **2008**, *21*, 515.
[27] B. Yang, I. Kwon, *Mol. Pharmaceutics* **2021**, *18*, 2397.
[28] C. T. Huynh, S. W. Kang, Y. Li, B. S. Kim, D. S. Lee, *Soft Matter* **2011**, *7*, 8984.
[29] D. Lee, N. Lee, I. Kwon, *Biomater. Sci.* **2018**, *6*, 2639.
[30] H. Xiong, Y. Zhou, Q. Zhou, D. He, S. Wan, Q. Tan, M. Zhang, X. Deng, J. Zhang, *ACS Appl. Mater. Interfaces* **2015**, *7*, 20255.